

Quark-Model Baryon-Baryon Interaction and its Applications to Hypernuclei ^{*})

Yoshikazu FUJIWARA, Choki NAKAMOTO^{*}, Yasuyuki SUZUKI^{**}, Michio KOHNO^{***}
and Kazuya MIYAGAWA ^{****}

Department of Physics, Kyoto University, Kyoto 606-8502, Japan

^{}Suzuka National College of Technology, Suzuka 510-0294, Japan*

*^{**}Department of Physics, Niigata University, Niigata 950-2181, Japan*

*^{***}Physics Division, Kyushu Dental College, Kitakyushu 803-8580, Japan*

*^{****}Department of Applied Physics, Okayama Science University, Okayama 700-0005, Japan*

The quark-model baryon-baryon interaction fss2, proposed by the Kyoto-Niigata group, is a unified model for the complete baryon octet ($B_8 = N, \Lambda, \Sigma$ and Ξ), which is formulated in a framework of the $(3q)$ - $(3q)$ resonating-group method (RGM) using the spin-flavor SU_6 quark-model wave functions and effective meson-exchange potentials at the quark level. Model parameters are determined to reproduce properties of the nucleon-nucleon system and the low-energy cross section data for the hyperon-nucleon scattering. Due to the several improvements including the introduction of vector-meson exchange potentials, fss2 has achieved very accurate description of the NN and YN interactions, comparable to various one-boson exchange potentials. We review the essential features of fss2 and our previous model FSS, and their predictions to few-body systems in confrontation with the available experimental data. Some characteristic features of the B_8B_8 interactions with the higher strangeness, $S = -2, -3, -4$, predicted by fss2 are discussed. These quark-model interactions are now applied to realistic calculations of few-body systems in a new three-cluster Faddeev formalism which uses two-cluster RGM kernels. As for the few-body systems, we discuss the three-nucleon bound states, the ΛNN - ΣNN system for the hypertriton, the $\alpha\alpha\Lambda$ system for ${}^9_\Lambda\text{Be}$, and the $\Lambda\Lambda\alpha$ system for ${}^6_{\Lambda\Lambda}\text{He}$.

§1. Introduction

An important purpose of studying baryon-baryon interactions in the quark model (QM) is to obtain the most accurate understanding of the fundamental strong interactions in a natural picture, in which the short-range part of the interaction is relevantly described by the quark-gluon degrees of freedom and the medium- and long-range parts by dominated meson-exchange processes. In the spin-flavor SU_6 QM, the baryon-baryon interactions for all the octet baryons ($B_8 = N, \Lambda, \Sigma$ and Ξ) are consistently treated with the well-known nucleon-nucleon (NN) interaction. We have recently proposed a comprehensive QM description of general baryon-octet baryon-octet (B_8B_8) interactions, which is formulated in the $(3q)$ - $(3q)$ resonating-group method (RGM) using the spin-flavor SU_6 QM wave functions, a colored version of the one-gluon exchange Fermi-Breit interaction, and effective meson-exchange potentials (EMEP's) acting between quarks.¹⁾⁻⁵⁾ The early version, the model FSS,¹⁾⁻³⁾ includes only the scalar (S) and pseudoscalar (PS) meson-exchange potentials as the

^{*}) Talk presented by Y. Fujiwara at the 18th Nishinomiya Yukawa Memorial Symposium on Strangeness in Nuclear Matter, 4 - 5 December 2003, Nishinomiya, Japan.

EMEP's, while the renovated one fss2^{4),5)} introduces also the vector (V) meson-exchange potentials and the momentum-dependent Bryan-Scott terms for the S and V mesons. Owing to these improvements, the model fss2 in the NN sector has attained the accuracy comparable to that of one-boson exchange potentials (OBEP's).

These QM potentials can now be used for various types of many-body calculations, which include the G -matrix calculations⁶⁾ of baryonic matter and the Faddeev calculations of few-baryon systems.⁷⁾ For this purpose, we have recently developed a new three-cluster formalism which uses two-cluster RGM kernels explicitly.⁸⁾ The proposed equation eliminates three-cluster redundant components by the orthogonality of the total wave function to the pairwise two-cluster Pauli-forbidden states. The explicit energy dependence inherent in the exchange RGM kernel is self-consistently determined. This equation is entirely equivalent to the Faddeev equation which uses a modified singularity-free T -matrix (which we call the RGM T -matrix) generated from the two-cluster RGM kernel. We first applied this formalism to a three-dineutron system and the 3α system, and obtained a complete agreement between the Faddeev calculations and variational calculations which use the translationally invariant harmonic-oscillator (h.o.) basis.^{8),9)} Here we apply the formalism to the Faddeev calculations of the three-nucleon ($3N$) bound state,⁷⁾ and the ΛNN - ΣNN system for the hypertriton, as well as the $\alpha\alpha\Lambda$ and $\Lambda\Lambda\alpha$ systems.

§2. Formulation

The present model is a low-energy effective model which introduces some of the essential features of QCD characteristics. The color degree of freedom of quarks is explicitly incorporated into the non-relativistic spin-flavor SU_6 quark model, and the full antisymmetrization of quarks is carried out in the RGM formalism. The gluon exchange effect is represented in the form of the quark-quark interaction. The confinement potential is a phenomenological r^2 -type potential, which has a favorable feature that it does not contribute to the baryon-baryon interactions. We use a color analogue of the Fermi-Breit (FB) interaction, motivated from the dominant one-gluon exchange process in conjunction with the asymptotic freedom of QCD. We postulate that the short-range part of the baryon-baryon interaction is well described by the quark degree of freedom. This includes the short-range repulsion and the spin-orbit force, both of which are successfully described by the FB interaction. On the other hand, the medium range attraction and the long-range tensor force, especially afforded by the pions, are extremely non-perturbative from the viewpoint of QCD. These are therefore most relevantly described by the effective meson exchange potentials (EMEP). In the previous model called FSS,¹⁾⁻³⁾ only the scalar and pseudoscalar mesons are introduced. The model fss2^{4),5)} is the most advanced model which also includes the vector-meson exchange EMEP. The full QM Hamiltonian H consists of the non-relativistic kinetic-energy term, the phenomenological confinement potential U_{ij}^{Cf} , the colored version of the full FB interaction U_{ij}^{FB} with explicit quark-mass dependence, and the EMEP U_{ij}^{Ω} generated from the scalar ($\Omega=S$), pseudoscalar (PS) and vector (V) meson exchange potentials acting between quarks:

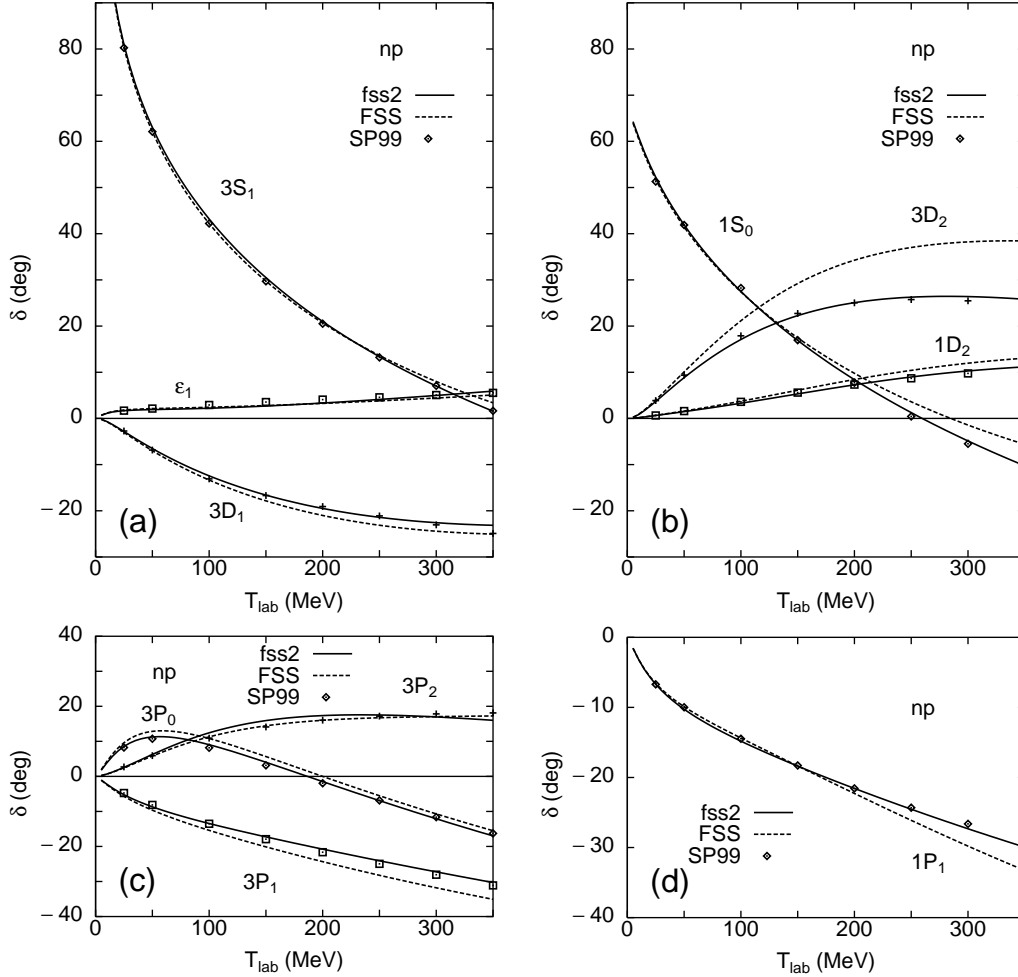


Fig. 1. Comparison of np phase-shift parameters for $J \leq 2$ with the phase-shift analysis SP99 by Arndt *et al.*¹²⁾ The solid curves are the results by fss2 and the dotted curves by FSS.

$$H = \sum_{i=1}^6 \left(m_i c^2 + \frac{\mathbf{p}_i^2}{2m_i} - T_G \right) + \sum_{i<j}^6 \left(U_{ij}^{\text{Cf}} + U_{ij}^{\text{FB}} + U_{ij}^{\text{S}} + U_{ij}^{\text{PS}} + U_{ij}^{\text{V}} \right). \quad (2.1)$$

The RGM equation for the relative-motion wave function $\chi(\mathbf{r})$ reads

$$\langle \phi(3q)\phi(3q) | E - H | \mathcal{A} \{ \phi(3q)\phi(3q)\chi(\mathbf{r}) \} \rangle = 0. \quad (2.2)$$

We solve this RGM equation in the momentum representation.¹⁰⁾ If we rewrite the RGM equation in the form of the Schrödinger-type equation as $[\varepsilon - H_0 - V_{\text{RGM}}(\varepsilon)] \times \chi(\mathbf{r}) = 0$, the potential term, $V_{\text{RGM}}(\varepsilon) = V_D + G + \varepsilon K$, becomes nonlocal and energy dependent. Here V_D represents the direct potential of EMEP's, G includes all the exchange kernels for the interaction and kinetic-energy terms, and K is the exchange

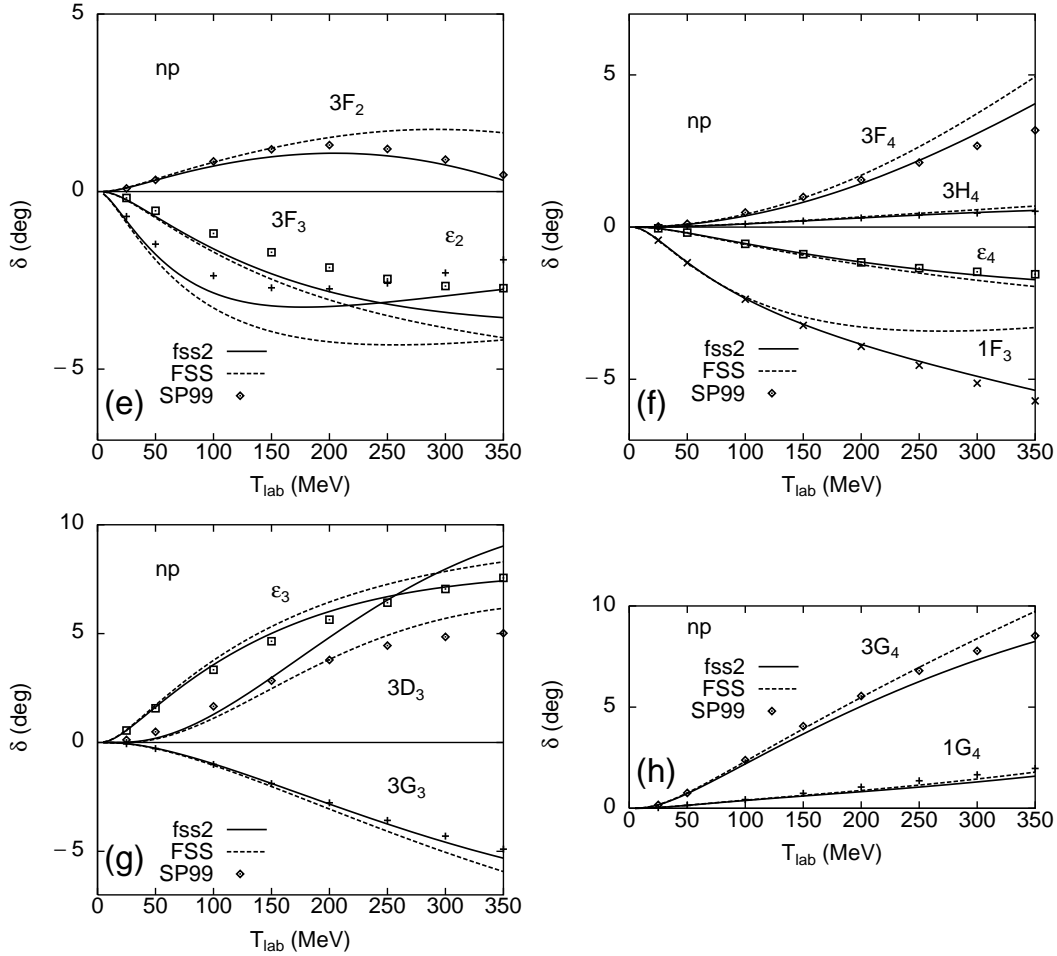


Fig. 2. Same as Fig. 1 but for the higher partial waves with $J \leq 4$.

normalization kernel. We calculate the plane-wave matrix elements of $V_{\text{RGM}}(\varepsilon)$, and set up with the Lippmann-Schwinger equation of the RGM T -matrix. This approach is convenient to proceed to the G -matrix calculations.^{6),11)} Faddeev calculations using these exchange kernels are also possible with some special considerations of the Pauli forbidden states.^{8),9)}

§3. B_8B_8 interactions by fss2 and FSS

3.1. NN properties and G -matrix calculations of nuclear matter

Figures 1 and 2 display some important low-partial wave NN phase-shift parameters predicted by the model fss2, in comparison with the phase shift analysis SP99.¹²⁾ The previous results by FSS are also shown with the dotted curves. Due to the inclusion of V mesons, the NN phase shifts of the fss2 at the non-relativistic energies up to $T_{\text{lab}} = 350$ MeV are greatly improved, and now have attained the

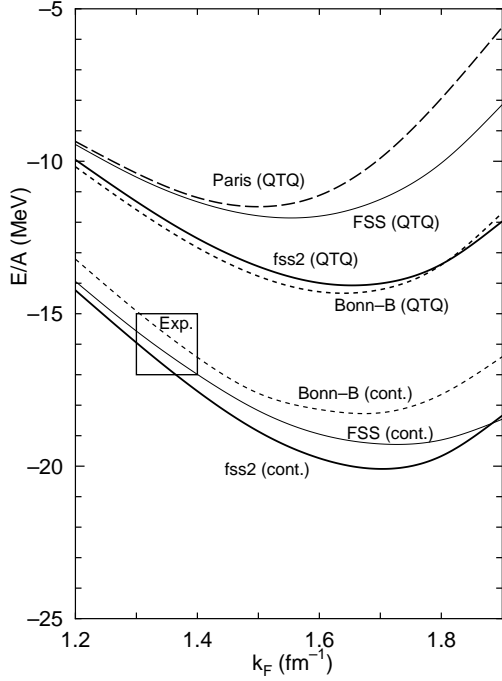


Fig. 3. Nuclear matter saturation curves obtained by fss2 and FSS, together with the results of the Paris potential¹⁷⁾ and the Bonn model-B potential.¹⁸⁾ The choice of the intermediate spectra is specified by “QTQ” and “cont.” The result for the Bonn-B potential in the continuous choice is taken from the non-relativistic calculation in Ref. 19).

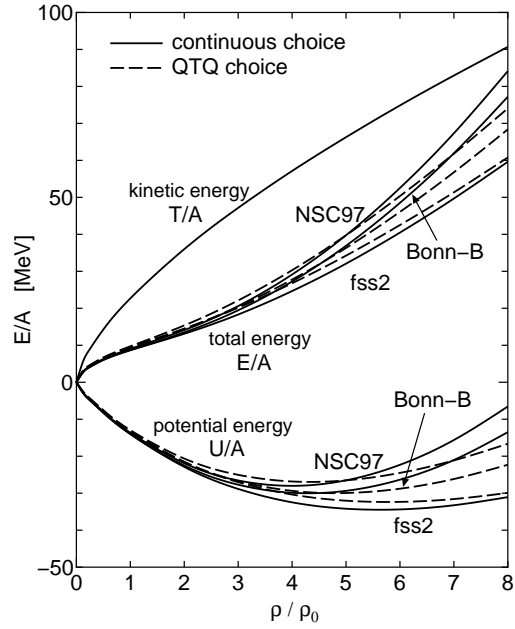


Fig. 4. Same as Fig. 3 but for the neutron matter saturation curve predicted by fss2. The normal density ρ_0 corresponds to the Fermi momentum $k_F^n = 1.35 \text{ fm}^{-1}$. The results of the Nijmegen soft-core potential (NSC97)²⁰⁾ and the Bonn-B potential¹⁸⁾ are also shown for comparison.

accuracy almost comparable to that of OBEP's. The good reproduction of the NN phase-shift parameters in fss2 continues up to $T_{\text{lab}} \sim 600 \text{ MeV}$,⁴⁾ where the inelasticity of the S -matrix becomes appreciable.

For the correct evaluation of the triton binding energy, it is well known that the proper reproduction of the deuteron D -state probability and the 1S_0 effective range

Table I. The deuteron properties by fss2 and FSS in the isospin basis. The results by the Bonn-B potential¹⁸⁾ are also shown for comparison. A small difference in FSS from Table IV of Ref. 2) is due to the numerical inaccuracy in the previous calculation. The effect of the meson exchange current is not included in the calculations of Q_d and μ_d .

	FSS	fss2	Bonn B	Expt.	Ref.
ϵ_d (MeV)	2.2561	2.2247	2.2246	2.224644 ± 0.000046	13)
P_D (%)	5.86	5.49	4.99	—	
$\eta = A_D/A_S$	0.0267	0.0253	0.0264	0.0256 ± 0.0004	14)
rms (fm)	1.963	1.960	1.968	1.9635 ± 0.0046	13)
Q_d (fm ²)	0.283	0.270	0.278	0.2860 ± 0.0015	15)
μ_d (μ_N)	0.8464	0.8485	0.8514	0.857406 ± 0.000001	16)

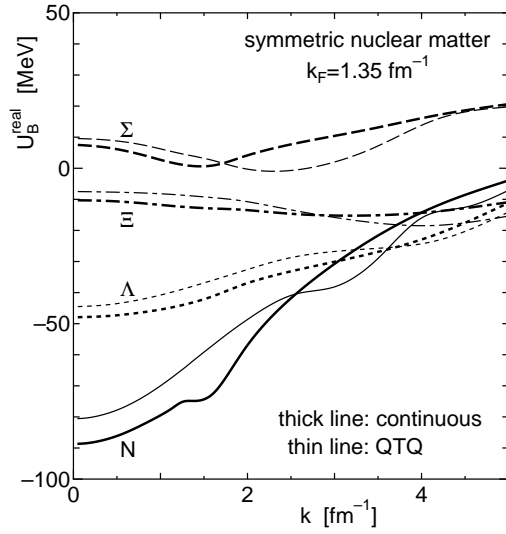


Fig. 5. The s.p. potentials $U_B(k)$ in symmetric nuclear matter, predicted by fss2, for the normal density ρ_0 with $k_F = 1.35 \text{ fm}^{-1}$.

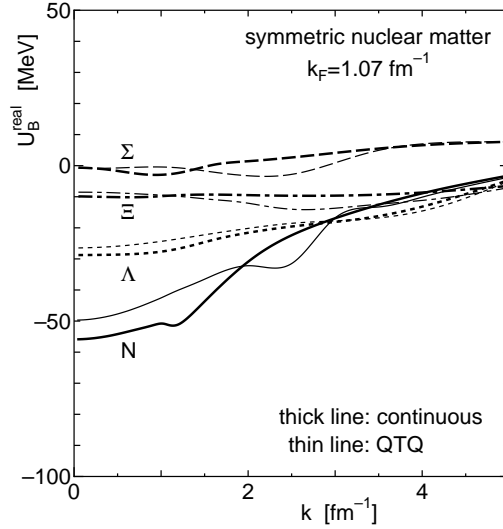


Fig. 6. Same as Fig. 5 but for half of the normal density ($\rho = 0.5 \rho_0$) with $k_F = 1.07 \text{ fm}^{-1}$.

parameters is essential. Table I shows the deuteron properties predicted by FSS and fss2, in comparison with the experiment. The predictions by the Bonn-B potential, which has a smaller deuteron D -state probability, is also shown for comparison.

Figure 3 shows saturation curves of symmetric nuclear matter, obtained by fss2 and FSS.⁶⁾ They depend on the prescription how one deals with the energy spectrum of the intermediate single-particle (s.p.) states. In both cases of the QTQ and the continuous choices, they are very similar to the predictions by meson exchange potentials. In the continuous choice, the saturation curves of fss2 and FSS are very similar to that of the Bonn-B potential.¹⁸⁾ Unfortunately, our results share the common unsatisfactory feature of any non-relativistic models, that the saturation point does not deviate from the Caester line.

The saturation curve for neutron matter, predicted by fss2, is also shown in Fig. 4. The results by the Nijmegen soft-core potential (NSC97)²⁰⁾ and the Bonn-B potential¹⁸⁾ are also shown for comparison. Since the strongly attractive ${}^3S_1 + {}^3D_1$ channel does not exist in this case, the total energy per neutron in neutron matter becomes repulsive in any models. We find that our quark model potential gives very similar results to the standard meson-exchange potentials, as long as the NN interaction is concerned.

The s.p. potentials of the nucleon and hyperons in symmetric nuclear matter are shown in Figs. 5 ($k_F = 1.35 \text{ fm}^{-1}$) and 6 ($k_F = 1.07 \text{ fm}^{-1}$) for the model fss2. For the standard Fermi momentum $k_F = 1.35 \text{ fm}^{-1}$, which corresponds to the normal density ρ_0 , these are fairly deep potentials. For the comparison with the depth of the s.p. potentials in the finite nuclei, one has to take a smaller value for k_F because of the surface effects. If we assume $k_F = 1.07 \text{ fm}^{-1}$, the s.p. potentials become much shallower, and the depth becomes almost comparable with the empirical values, -50

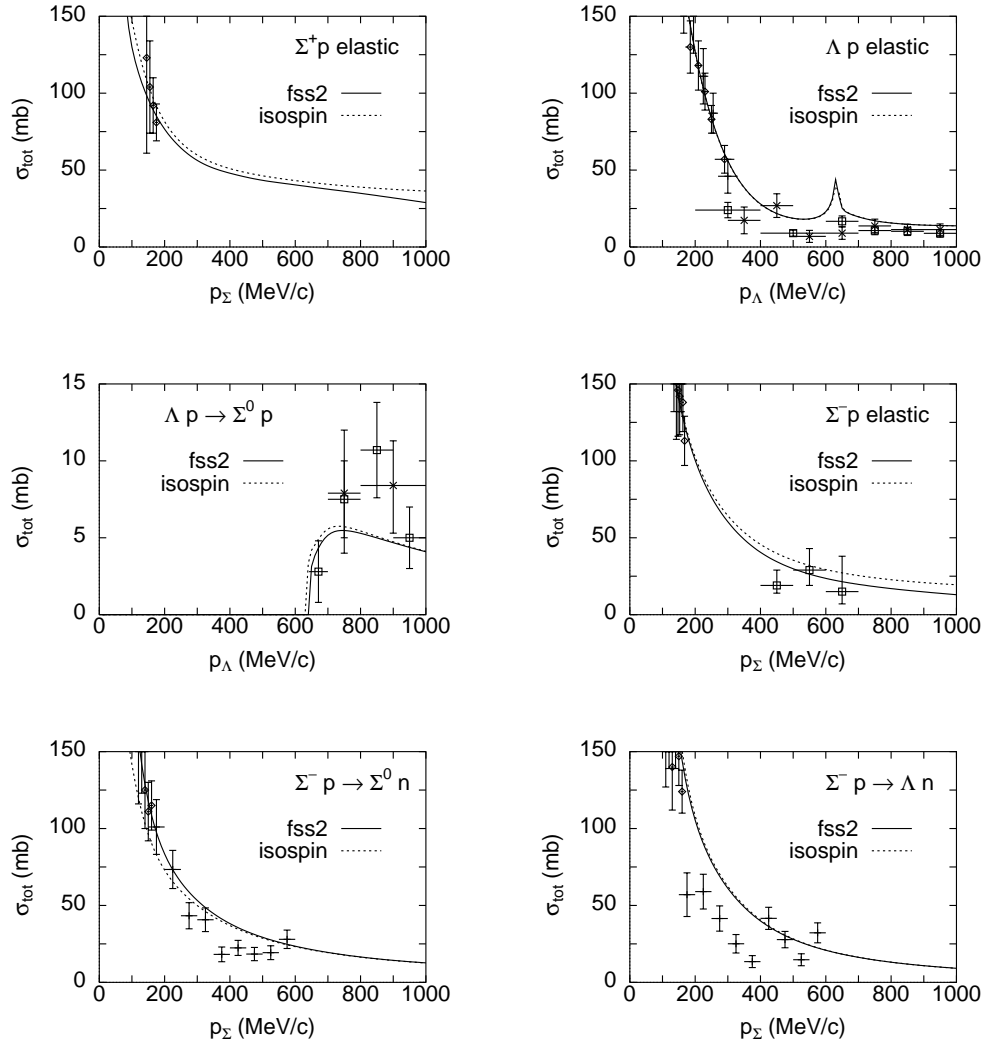


Fig. 7. Calculated YN total cross sections compared with the available experimental data.

MeV for N , -30 MeV for Λ , and $-10 \sim -14$ MeV for Ξ . The sign of the Σ s.p. potential is still controversial.

3.2. YN and YY interactions by $fss2$ and FSS

The total cross sections of the hyperon-nucleon (YN) scattering predicted by $fss2$ are compared with the available experimental data in Fig. 7. The “total” cross sections for the scattering of charged particles (i.e., Σ^+p and Σ^-p systems) are calculated by integrating the differential cross sections over $\cos\theta_{\min} = 0.5 \sim \cos\theta_{\max} = -0.5$. The solid curves indicate the result in the particle basis, while the dashed curves in the isospin basis. In the latter case, the effects of the charge symmetry breaking, such as the Coulomb effect and the small difference of the threshold energies for Σ^-p and Σ^0n channels, are neglected. New experimental data for Σ^-p

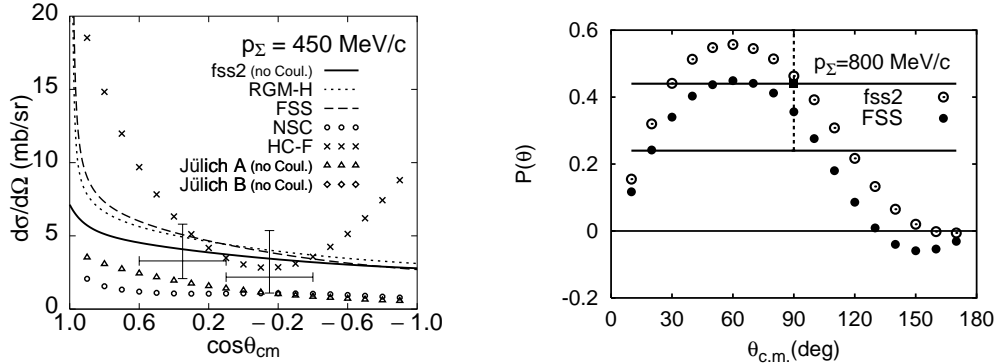


Fig. 8. Left: Σ^+p differential cross sections at $p_\Sigma = 450$ MeV/ c predicted by various models. The experimental data are cited from Ref. 22). Right: Σ^+p polarization at $p_\Sigma = 800$ MeV/ c , predicted by fss2 and FSS. The experimental data are cited from Ref. 23).

elastic total cross sections at the intermediate energies, $p_\Sigma = 400$ - 700 MeV/ c , measured at KEK,²¹⁾ are consistent with the fss2 predictions.

The Σ^+p differential cross sections at the intermediate energy $p_\Sigma = 450$ MeV/ c are compared with the KEK experiment²²⁾ in the left panel of Fig. 8. We need more experimental data to increase the statistics, in order to see which model is the most appropriate. In the right panel, the polarization observables for the Σ^+p elastic scattering at $p_\Sigma = 800$ MeV/ c are shown for the models fss2 and FSS. The recent experimental data from KEK-PS 457²³⁾ imply the asymmetry parameter $a^{\text{exp}} = 0.44 \pm 0.2$ at $p_\Sigma = 800 \pm 200$ MeV/ c , which is not inconsistent with our quark-model predictions although the specific scattering angle is not possible to be identified.

We show some comparison of the Ξ^-N total cross sections which are recently obtained from the BNL-E906 experiment.²⁴⁾ The in-medium Ξ^-N total cross sections around the momentum region $p_{\text{lab}} \sim 550$ MeV/ c are estimated as $\sigma_{\Xi N}(\text{in medium}) = 30 \pm 6.7_{-3.6}^{+3.7}$ mb. More detailed analysis using the Eikonal approximation²⁵⁾ gives $\sigma_{\Xi N}(\text{in medium}) = 20.9 \pm 4.5_{-2.4}^{+2.5}$ mb. They have also estimated the cross section ratio $\sigma_{\Xi^-p}/\sigma_{\Xi^-n} = 1.1_{-0.7}^{+1.4} \pm 0.7_{-0.4}$. If we compare these experimental data with the FSS and fss2 predictions depicted in Fig. 9, we find that the FSS predictions in the left panels seem to be more favorable. However, we definitely need more experimental data with higher statistics.

3.3. Characteristics of the B_8B_8 Interactions by fss2

Since our quark-model parameters are fixed by using the experimental data in the NN and YN sectors, the B_8B_8 interactions beyond the strangeness $S = -1$ are all model predictions.⁵⁾ For the systematic understanding of these interactions, it is convenient to discuss them by using the SU_3 representation basis for the two-baryon systems. This is because the quark-model Hamiltonian is approximately SU_3 scalar, and the interactions with the same SU_3 label ($\lambda\mu$) should have very similar characteristics, as long as the flavor symmetry breaking is negligible. Table II illustrates how the two baryon systems in the isospin basis are classified as the

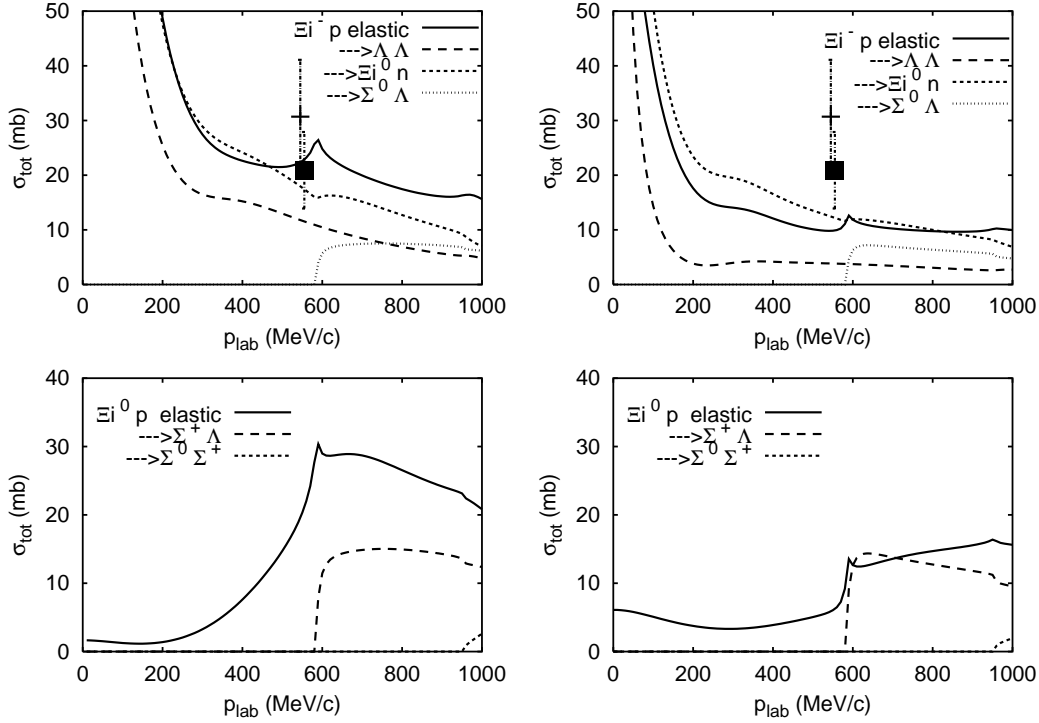


Fig. 9. Ξ^-p and Ξ^0p total cross sections predicted by FSS (left) and fss2 (right). For Ξ^-p cross sections both of the isospin $I = 0$ and 1 channels contribute, while for Ξ^-n (or Ξ^0p) only the channel with $I = 1$ contributes. The Coulomb force is neglected.

superposition of the SU_3 basis. It has entirely different structure between the flavor symmetric and antisymmetric cases. In the 1S_0 state, for example, there appear many states having the dominant (22) components. The S -state B_8B_8 interactions for these states should be very similar to that for the NN 1S_0 state. The $(11)_s$ component is completely Pauli forbidden and is characterized by the strong repulsion originating from the quark Pauli principle. The (00) component in the H-particle channel is attractive from the color-magnetic interaction. On the other hand, in the NN sector the 3S_1 state with $I = 0$ is composed of the pure (03) state, and the deuteron is bound in this channel owing to the strong one-pion tensor force. This SU_3 state in the flavor antisymmetric case is converted to the (30) state in the larger side of the strangeness. Since the (30) state is almost Pauli forbidden, the interaction is strongly repulsive. Therefore, the $\Xi\Xi$ interaction is not so attractive as NN , since they are combinations of (22) and (30) . The other SU_3 state $(11)_a$ turns out to have very weak interaction. After all, the strangeness $S = -2$ sector is most difficult, since it is a turning point of the strangeness. It is also interesting to see that $\Xi\Sigma$ channel with $I = 3/2$ should be fairly attractive, since the same (22) and (03) SU_3 states as in the NN system appear in this isospin channel.

Figure 10 shows fss2 predictions of the 1S_0 phase shifts for various B_8B_8 interactions having the pure (22) configuration. Although the $\Sigma\Sigma$ interaction with the isospin $I = 2$ is very similar to the NN interaction, the other interactions generally

get weaker as the strangeness involved becomes larger. This is a combined effect of the flavor symmetry breaking in the quark and meson-exchange contributions. In particular, the $\Xi\Xi$ interaction has the lowest rise of the phase shift, which is less than 30° . Accordingly, the the $\Xi\Xi$ total cross sections become much smaller than the other systems. We find that the NN interaction is the strongest and has the largest cross sections among any combinations of the octet baryons.

Figure 11 shows the 1S_0 phase shift curves, predicted by fss2, in the $\Lambda\Lambda$ - ΞN - $\Sigma\Sigma$ coupled-channel system with the isospin $I = 0$. The maximum peak of the $\Lambda\Lambda$ phase shift is less than 20° , which is much smaller than the previous predictions by various models. This result is in good agreement with the recent experimental data for the double Λ hypernucleus ${}^6_{\Lambda\Lambda}\text{He}$. The finding of this event, called the Nagara event,²⁶⁾ is one of the most important contributions in recent years, since the assignment of the decaying scheme is very definite. The $\Delta B_{\Lambda\Lambda}$ value, defined by $\Delta B_{\Lambda\Lambda} = B_{\Lambda\Lambda}({}^6_{\Lambda\Lambda}\text{He}) - 2B_{\Lambda}({}^5_{\Lambda}\text{He})$, is deduced from this event as $\Delta B_{\Lambda\Lambda} = 1.01 \pm 0.20$ MeV, which implies a weak attraction for the $\Lambda\Lambda$ interaction. Our G -matrix calculation of this system yields an almost right answer, $\Delta B_{\Lambda\Lambda} = 1.12 \sim 1.24$ MeV, by taking into account the important contribution from the α -particle rearrangement energy.²⁷⁾ In

Table II. The relationship between the isospin basis and the flavor- SU_3 basis for the $B_8 B_8$ systems. The flavor- SU_3 symmetry is given by the Elliott notation $(\lambda\mu)$. The heading \mathcal{P} denotes the flavor exchange symmetry, S the strangeness, and I the isospin.

S	$B_8 B_8 (I)$	$\mathcal{P} = +1$ (symmetric)		$\mathcal{P} = -1$ (antisymmetric)	
		1E	or 3O	3E	or 1O
0	$NN (0)$	-		(03)	
	$NN (1)$	(22)		-	
-1	$\Lambda N (1/2)$	$\frac{1}{\sqrt{10}}[(11)_s + 3(22)]$		$\frac{1}{\sqrt{2}}[-(11)_a + (03)]$	
	$\Sigma N (1/2)$	$\frac{1}{\sqrt{10}}[3(11)_s - (22)]$		$\frac{1}{\sqrt{2}}[(11)_a + (03)]$	
	$\Sigma N (3/2)$	(22)		(30)	
-2	$\Lambda\Lambda (0)$	$\frac{1}{\sqrt{5}}(11)_s + \frac{9}{2\sqrt{30}}(22) + \frac{1}{2\sqrt{2}}(00)$		-	
	$\Xi N (0)$	$\frac{1}{\sqrt{5}}(11)_s - \sqrt{\frac{3}{10}}(22) + \frac{1}{\sqrt{2}}(00)$		(11) _a	
	$\Xi N (1)$	$\sqrt{\frac{3}{5}}(11)_s + \sqrt{\frac{2}{5}}(22)$		$\frac{1}{\sqrt{3}}[-(11)_a + (30) + (03)]$	
	$\Sigma\Lambda (1)$	$-\sqrt{\frac{2}{5}}(11)_s + \sqrt{\frac{3}{5}}(22)$		$\frac{1}{\sqrt{2}}[(30) - (03)]$	
	$\Sigma\Sigma (0)$	$\sqrt{\frac{3}{5}}(11)_s - \frac{1}{2\sqrt{10}}(22) - \sqrt{\frac{3}{8}}(00)$		-	
	$\Sigma\Sigma (1)$	-		$\frac{1}{\sqrt{6}}[2(11)_a + (30) + (03)]$	
	$\Sigma\Sigma (2)$	(22)		-	
-3	$\Xi\Lambda (1/2)$	$\frac{1}{\sqrt{10}}[(11)_s + 3(22)]$		$\frac{1}{\sqrt{2}}[-(11)_a + (30)]$	
	$\Xi\Sigma (1/2)$	$\frac{1}{\sqrt{10}}[3(11)_s - (22)]$		$\frac{1}{\sqrt{2}}[(11)_a + (30)]$	
	$\Xi\Sigma (3/2)$	(22)		(03)	
-4	$\Xi\Xi (0)$	-		(30)	
	$\Xi\Xi (1)$	(22)		-	

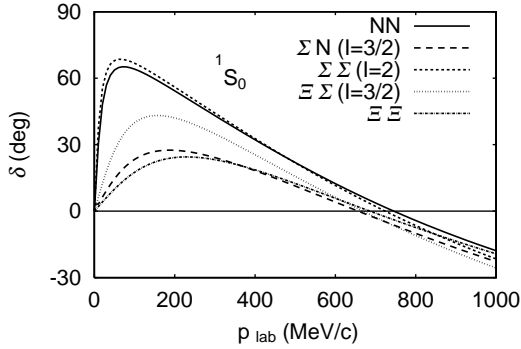


Fig. 10. 1S_0 phase shifts for various B_8B_8 interactions with the pure (22) state. The model is fss2.

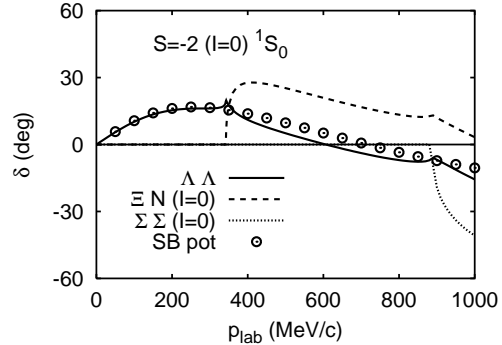


Fig. 11. 1S_0 phase shifts, predicted by fss2, in the $\Lambda\Lambda$ - ΞN - $\Sigma\Sigma$ coupled-channel system with the isospin $I = 0$. The single-channel phase shift of the $\Lambda\Lambda$ channel, predicted by the SB potential, is also shown in circles.

the next section, we will solve the Faddeev equation of the $\Lambda\Lambda\alpha$ system, by using the $\Lambda\Lambda$ T -matrix predicted by our QM interaction.

Some of the following characteristics of fss2 for the B_8B_8 interactions are very much different from the Nijmegen predictions given by Stoks and Rijken.²⁸⁾

- There is no bound state in the B_8B_8 system, except for the deuteron.
- The $\Xi\Xi$ total cross sections are not so large as the NN total cross sections.
- The ΞN interaction has a strong isospin dependence like the ΣN interaction.
- The $\Xi^-\Sigma^-$ (namely, $\Xi\Sigma(I = 3/2)$) interaction is fairly attractive.

§4. Faddeev calculation

4.1. Three-nucleon bound state

Since our QM B_8B_8 interaction describes the short-range repulsion very differently from the meson-exchange potentials, it is interesting to examine the three-nucleon system predicted by fss2 and FSS. Here we solve the Faddeev equation for ^3H , by directly using the QM RGM kernel in the isospin basis.⁷⁾ Our Faddeev calculation is the full 50-channel calculation up to the maximum angular momentum $J = 6$, and the values are almost completely converged as seen in Table III.²⁹⁾ The fss2 prediction, -8.52 MeV, seems to be overbound in comparison with the experimental value $E^{\text{exp}}(^3\text{H}) = -8.48$ MeV. In fact, this is not the case, since all these calculations neglect the charge dependence of the NN interaction, in which the 1S_0 interaction of the nn system is less attractive than that of the np system. The effect of the charge dependence is estimated to be -0.19 MeV for the triton binding energy.¹⁸⁾ If we take this into account, our result is still 150 keV less bound. If we attribute this difference to the effect of the three-nucleon force, it is by far smaller than the generally accepted values, $0.5 \sim 1$ MeV,³⁰⁾ predicted by many Faddeev calculations employing modern realistic meson-theoretical NN interactions. The charge root-mean-square radii of ^3H and ^3He are correctly reproduced. An important point

Table III. The three-nucleon bound state properties predicted by the Faddeev calculation with fss2 and FSS. The np interaction is used in the isospin basis. The heading ‘‘No. of channels’’ implies the number of two-nucleon channels included; n_{\max} is the dimension of the diagonalization for the Faddeev equation; ε_{NN} is the NN expectation value determined self-consistently; $E(^3\text{H})$ is the ground-state energy; and $\sqrt{\langle r^2 \rangle_{^3\text{H}}} (\sqrt{\langle r^2 \rangle_{^3\text{He}}})$ is the charge rms radius for ^3H (^3He), including the proton and neutron size corrections. The Coulomb force and the relativistic corrections are neglected.

model	No. of channels	n_{\max}	ε_{NN} (MeV)	$E(^3\text{H})$ (MeV)	$\sqrt{\langle r^2 \rangle_{^3\text{H}}}$ (fm)	$\sqrt{\langle r^2 \rangle_{^3\text{He}}}$ (fm)
fss2	2 (S)	2,100	2.361	-7.807	1.80	1.96
	5 (SD)	5,250	4.341	-8.189	1.75	1.92
	10 ($J \leq 1$)	10,500	4.249	-8.017	1.76	1.94
	18 ($J \leq 2$)	18,900	4.460	-8.439	1.72	1.90
	34 ($J \leq 4$)	35,700	4.488	-8.514	1.72	1.90
	50 ($J \leq 6$)	112,500	4.492	-8.519	1.72	1.90
FSS	2 (S)	2,100	2.038	-7.675	1.83	1.99
	5 (SD)	5,250	3.999	-8.034	1.78	1.95
	10 ($J \leq 1$)	10,500	3.934	-7.909	1.78	1.97
	18 ($J \leq 2$)	18,900	4.160	-8.342	1.74	1.93
	34 ($J \leq 4$)	35,700	4.175	-8.390	1.74	1.92
	50 ($J \leq 6$)	112,500	4.177	-8.394	1.74	1.92

here is that we can reproduce enough binding energy of the triton, without reducing the deuteron D -state probability.

The self-consistent energy of the two-cluster RGM kernel, ε_{NN} , has a clear physical meaning related to the decomposition of the total triton energy E into the kinetic-energy and potential-energy contributions: $\varepsilon_{NN} = E/3 + \langle H_0 \rangle/6$. Table IV shows this decomposition, together with the results of CD-Bonn and AV18 potentials.³⁰⁾ We find that our quark model results by FSS and fss2 are just middle between these potentials, which have very different strengths of the tensor force.

4.2. The hypertriton

Next, we apply our QM NN and YN interactions to the hypertriton ($^3_\Lambda\text{H}$) with the small separation energy of the Λ -particle, $B_\Lambda^{\text{exp}} = 130 \pm 50$ keV.³¹⁾ Since the Λ -particle is far apart from the two-nucleon subsystem, the on-shell properties of

Table IV. Decomposition of the total triton energy E into the kinetic-energy and potential-energy contributions: $E = \langle H_0 \rangle + \langle V \rangle$. The unit is in MeV. In the present framework, this is given by the expectation value ε_{NN} of the two-cluster Hamiltonian with respect to the Faddeev solution, which is determined self-consistently. The results of CD-Bonn and AV18 are taken from Ref. 30).

model	ε_{NN}	E	$\langle H_0 \rangle$	$\langle V \rangle$
fss2	4.492	-8.519	43.99	-52.51
FSS	4.177	-8.394	41.85	-50.25
CD-Bonn	3.566	-8.012	37.42	-45.43
AV18	5.247	-7.623	46.73	-54.35

Table V. Results of the hypertriton Faddeev calculations by fss2 and FSS. The heading E is the hypertriton energy measured from the ΛNN threshold; B_Λ is the Λ separation energy; ε_{NN} ($\varepsilon_{\Lambda N}$) is the NN (ΛN) expectation value determined self-consistently; and P_Σ is the ΣNN probability in percent. The norm of admixed redundant components is less than 10^{-9} .

model	No. of channels	E (MeV)	B_Λ (keV)	ε_{NN} (MeV)	$\varepsilon_{\Lambda N}$ (MeV)	P_Σ (%)
fss2	6 (S)	-2.362	137	-1.815	3.548	0.450
	15 (SD)	-2.423	198	-1.762	5.729	0.652
	30 ($J \leq 1$)	-2.403	178	-1.786	5.664	0.615
	54 ($J \leq 2$)	-2.498	273	-1.673	5.974	0.777
	102 ($J \leq 4$)	-2.513	288	-1.658	6.022	0.804
	150 ($J \leq 6$)	-2.514	289	-1.657	6.024	0.805
FSS	6 (S)	-2.910	653	-1.309	3.984	1.022
	15 (SD)	-2.967	710	-1.433	6.171	1.200
	30 ($J \leq 1$)	-2.947	691	-1.427	6.143	1.191
	54 ($J \leq 2$)	-3.121	865	-1.323	6.467	1.348
	102 ($J \leq 4$)	-3.134	877	-1.317	6.488	1.360
	150 ($J \leq 6$)	-3.134	878	-1.317	6.488	1.361

the ΛN and ΣN interactions are expected to be well reflected in this system. In particular, this system is very useful to learn the relative strength of 1S_0 and 3S_1 attractions of the ΛN interaction, since the 1S_0 component plays a more important role than 3S_1 in this system and the available low-energy Λp total cross section data cannot discriminate many possible combinations of the 1S_0 and 3S_1 interactions. In fact, Ref. 32)–34) showed that most meson-theoretical interactions fail to bind the hypertriton, except for the Nijmegen soft-core potentials NSC89,³⁵⁾ NSC97f and NSC97e.²⁰⁾ It is also pointed out in Refs. 32) and 34) that a small admixture of the ΣNN components less than 1% is very important for this binding. We therefore carry out the ΛNN - ΣNN coupled-channel Faddeev calculation, by properly taking into account the existence of the SU_3 Pauli forbidden state $(11)_s$ at the quark level.

Table V shows the results of the Faddeev calculations using fss2 and our previous model FSS. In the 15-channel calculation including the S and D waves of the NN and YN interactions, we have already obtained $B_\Lambda = -\varepsilon_d - E(^3\Lambda\text{H}) \sim 200$ keV for fss2. The convergence with the extension to the higher partial waves is very rapid, and the total angular-momentum of the baryon pairs with $J \leq 4$ is good enough for 1 keV accuracy. As for the converged B_Λ values with 150-channel ΛNN and ΣNN configurations, we obtain $B_\Lambda = 289$ keV and the ΣNN component $P_\Sigma = 0.80\%$ for the fss2 prediction, and $B_\Lambda = 878$ keV and $P_\Sigma = 1.36\%$ for FSS.

Table VI shows the correlation between the Λ separation energy B_Λ and the 1S_0 and 3S_1 effective range parameters of FSS, fss2 and NSC89 ΛN interactions. Although all of these ΛN interactions reproduce the low-energy ΛN total cross section data below $p_\Lambda \sim 300$ MeV/ c within the experimental error bars, our quark-model interactions seem to be slightly more attractive than the Nijmegen soft-core potential NSC89.³⁵⁾ The model FSS gives a large overbinding since the 1S_0 ΛN

Table VI. 1S_0 and 3S_1 effective range parameters of various ΛN interactions and the Λ separation energy B_Λ of the hypertriton. The B_Λ value for NSC89 is taken from Ref. 34).

model	a_s (fm)	r_s (fm)	a_t (fm)	r_t (fm)	B_Λ (keV)
FSS ²⁾	-5.41	2.26	-1.03	4.20	878
fss2 ^{4), 5)}	-2.59	2.83	-1.60	3.01	289
NSC89 ³⁵⁾	-2.78	2.88	-1.41	3.11	143

interaction is strongly attractive. The phase-shift difference of the 1S_0 and 3S_1 states at $p_\Lambda \sim 200$ MeV/ c is $\delta(^1S_0) - \delta(^3S_1) \sim 29^\circ$ for FSS, while $\sim 7^\circ$ for fss2. Since the present fss2 result is still slightly overbound, this difference should be somewhat smaller in order to reproduce the correct experimental value $B_\Lambda^{\text{exp}} = 130 \pm 50$ keV. From the two results given by fss2 and FSS, we can extrapolate the desired difference to be $0^\circ \sim 2^\circ$, which is consistent with the result in Ref. 36) using simulated interactions of the Nijmegen models.

Table V also shows that the expectation value of the NN Hamiltonian, ε_{NN} , determined self-consistently is rather close to the deuteron energy $-\varepsilon_d$, especially in fss2. This feature is even marked if we decompose these energies to the kinetic-energy and potential-energy contributions. Table VII shows this decomposition with respect to fss2, FSS and NSC89. (For this comparison, we use the definition of the kinetic-energy part of the deuteron, given by $h_d = \langle \chi_d | h_{NN} | \chi_d \rangle / \langle \chi_d | \chi_d \rangle$, where χ_d is the RGM relative wave function between the neutron and the proton.) In fss2, the kinetic-energy of the NN subsystem is 1.88 MeV larger than that of the deuteron, which implies that the NN subsystem shrinks by the effect of the outer Λ -particle, in comparison with the deuteron in the free space. In NSC89, this difference is even smaller; i.e., 1.18 MeV. These results are consistent with the fact that the hypertriton in NSC89 is more loosely bound ($B_\Lambda = 143$ keV)³⁴⁾ than in fss2 (289 keV), and the Λ -particle is very far apart from the NN cluster. The ΣNN probability in NSC89 is $P_\Sigma = 0.5\%$.³²⁾ Table VII also lists the kinetic-energy and potential-energy decompositions for the ΛN - ΣN averaged YN expectation value ε_{YN} and the total energy E . The kinetic energies of ε_{YN} are much smaller than those of

Table VII. Decomposition of the NN and YN expectation values (ε_{NN} and ε_{YN}), the deuteron energy ($-\varepsilon_d$) and the total three-body energy E to the kinetic-energy and potential-energy contributions. The unit is in MeV. The results for NSC89 are taken from Ref. 32).

model	$h_{NN} + V_{NN} = \varepsilon_{NN}$	$h_d + V_d = -\varepsilon_d$ (deuteron)
FSS	19.986 - 21.303 = -1.317	16.982 - 19.238 = -2.256
fss2	19.376 - 21.032 = -1.657	17.495 - 19.720 = -2.225
NSC89	20.48 - 22.25 = -1.77	19.304 - 21.528 = -2.224
model	$h_{YN} + V_{YN} = \varepsilon_{YN}$	$\langle H \rangle + \langle V \rangle = E$
FSS	10.036 - 4.602 = 5.435	27.372 - 30.506 = -3.134
fss2	8.071 - 2.671 = 5.401	23.860 - 26.374 = -2.514
NSC89	7.44 - 3.54 = 3.90	23.45 - 25.79 = -2.34

ε_{NN} , which indicates that the relative wave functions between the hyperon and the nucleon are widely spread in the configuration space. The comparison of the total-energy decomposition shows that the wave functions of fss2 and NSC89 may be very similar. A clear difference between fss2 and NSC89 appears in the roles of higher partial waves. The energy increase due to the higher partial waves than the S and D waves is 91 keV in fss2 and 168 keV in FSS, respectively. On the other hand, the results in Refs. 32) and 34) imply that this is only 20 - 30 keV in the case of NSC89. This difference can originate from both of the NN and YN interactions. Since the characteristics of the meson-theoretical YN interactions in higher partial waves are a priori unknown, more detailed analysis of the fss2 results might shed light on the adequacy of the quark-model baryon-baryon interactions.

4.3. The $\alpha\alpha\Lambda$ system for ${}^9_{\Lambda}\text{Be}$

As another typical example of three-cluster systems composed of two identical clusters, we apply the present formalism to the $\alpha\alpha\Lambda$ Faddeev calculation for ${}^9_{\Lambda}\text{Be}$, using the $\alpha\alpha$ RGM kernel and the $\Lambda\alpha$ folding potential generated from a simple ΛN effective interaction.³⁷⁾ For the $\alpha\alpha$ RGM kernel, we use the the three-range Minnesota force³⁸⁾ with the Majorana exchange mixture $u = 0.94687$, and the h.o. width parameter, $\nu = 0.257 \text{ fm}^{-2}$, assumed for the $(0s)^4$ α -clusters. The $\alpha\alpha$ phase shifts are nicely reproduced in the $\alpha\alpha$ RGM calculation, using this effective NN interaction. For the 3α system, we find that the ground-state energy obtained by solving the present 3α Faddeev equation is only 1.8 MeV higher than that of the fully microscopic 3α RGM calculation. The effective ΛN interaction, denoted by SB (Sparenberg-Baye potential) in Table VIII, is constructed from the 1S_0 and 3S_1 phase shifts predicted by the YN sector of the model fss2, by using an inversion method based on supersymmetric quantum mechanics.³⁹⁾ These are simple two-range Gaussian potentials which reproduce the low-energy behavior of the ΛN phase shifts in Fig. 12, obtained in the full coupled-channel calculations:

$$\begin{aligned} V_{1S_0}(r) &= -128.0 \exp(-0.8908 r^2) + 1015 \exp(-5.383 r^2) \quad , \\ V_{3S_1}(r) &= -56.31 f \exp(-0.7517 r^2) + 1072 \exp(-13.74 r^2) \quad , \end{aligned}$$

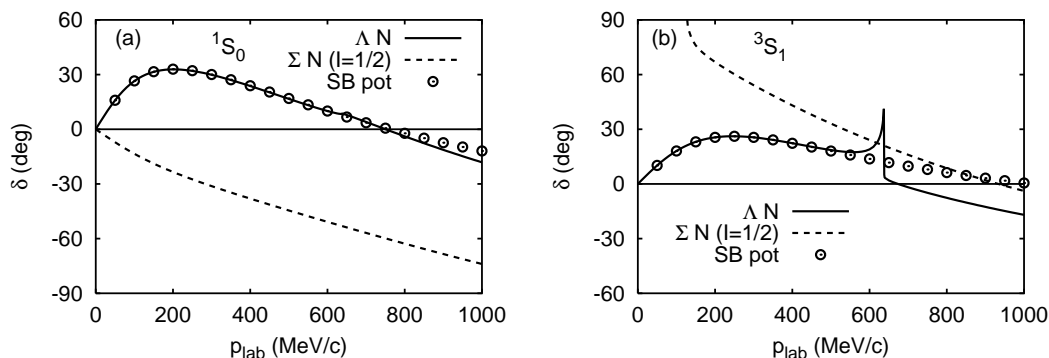


Fig. 12. ΛN - ΣN 1S_0 (a) and 3S_1 (b) phase shifts for the isospin $I = 1/2$ channel, calculated with fss2 (solid and dashed curves) and with the SB potential (circles).

Table VIII. The ground-state energy $E_{\text{gr}}(0^+)$ and 2^+ excitation energy $E_x(2^+)$ in MeV, calculated by solving the Faddeev equation for the $\alpha\alpha\Lambda$ system in the LS coupling scheme. The $\alpha\alpha$ RGM kernel is generated from the three-range Minnesota force. The ΛN force, SB, stands for the Sparenberg-Baye potential and NS - JB are the G -matrix based effective forces used by Hiyama *et al.*⁴²⁾ In Ref. 42), the orthogonality condition model (OCM) is used for the $\alpha\alpha$ interaction. The experimental values are cited from Ref. 43).

$V_{\Lambda N}$	$E_{\text{gr}}(0^+)$ (MeV)		$E_x(2^+)$ (MeV)
	present	Ref. 42)	
SB	-6.837	-	2.915
NS	-6.742	-6.81	2.916
ND	-7.483	-7.57	2.935
NF	-6.906	-7.00	2.930
JA	-6.677	-6.76	2.919
JB	-6.474	-6.55	2.911
Exp't	-6.62 ± 0.04		3.029(3)
			3.060(3)

where $V(r)$ in MeV and r in fm is the relative distance between Λ and N . In the 3S_1 state, the phase-shift behavior only in the low-momentum region with $p_{\text{lab}} < 600$ MeV/ c is fitted, since the cusp structure is never reproduced in the single-channel calculation. Since any central and single-channel effective ΛN force leads to the well-known overbinding problem of ${}^5_\Lambda\text{He}$ by about 2 MeV (in the present case, it is 1.63 MeV),⁴⁰⁾ the attractive part of the 3S_1 ΛN potential is modified to reproduce the correct binding energy, $E^{\text{exp}}({}^5_\Lambda\text{He}) = -3.12 \pm 0.02$ MeV, with an adjustable parameter $f = 0.8923$. This overbinding problem is mainly attributed to the Brueckner rearrangement effect of the α -cluster, originating from the starting energy dependence of the bare two-nucleon interaction due to the addition of an extra Λ particle.⁴¹⁾ The odd-state ΛN interaction is assumed to be zero. All partial waves up to $\lambda_{\text{Max}} = \ell_{1\text{Max}} = 6$ for the $\alpha\alpha$ and $\Lambda\alpha$ pairs are included. The direct and exchange Coulomb kernel between the two α -clusters is introduced at the nucleon level with the cut-off radius, $R_C = 14$ fm. Table VIII shows the ground-state (0^+) and the 2^+ excitation energies of ${}^9_\Lambda\text{Be}$, predicted by the SB and the other various ΛN potentials used by Hiyama *et al.*⁴²⁾ In the present calculations using only the central force, the SB potential with the pure Serber character can reproduce the the ground-state and the excitation energies within 100 - 200 keV accuracy.

4.4. The $\Lambda\Lambda\alpha$ system for ${}^6_{\Lambda\Lambda}\text{He}$

We can use the $\Lambda\alpha$ T -matrix, used in the $\alpha\alpha\Lambda$ Faddeev calculation, to calculate the ground-state energy of ${}^6_{\Lambda\Lambda}\text{He}$. The full coupled-channel T -matrices of fss2 and FSS with the strangeness $S = -2$ and the isospin $I = 0$ are employed for the $\Lambda\Lambda$ RGM T -matrix. Table IX shows the $\Delta B_{\Lambda\Lambda}$ values in MeV, predicted by various combinations of the ΛN and $\Lambda\Lambda$ interactions. The results of a simple three-range Gaussian potential, $V_{\Lambda\Lambda}$ (Hiyama), used in Ref. 42) are also shown. We find that this $\Lambda\Lambda$ potential and our Faddeev calculation using the FSS T -matrix yield very similar results with the large $\Delta B_{\Lambda\Lambda}$ values about 3.6 MeV, since the $\Lambda\Lambda$ phases

Table IX. Comparison of $\Delta B_{\Lambda\Lambda}$ values in MeV, predicted by various $\Lambda\Lambda$ interactions and $V_{\Lambda N}$ potentials. The $\Lambda\Lambda$ potential $V_{\Lambda\Lambda}$ (Hiyama) is the three-range Gaussian potential used in Ref. 42). FSS and fss2 use the $\Lambda\Lambda$ RGM T -matrix in the free space. The heading $\varepsilon_{\Lambda\Lambda}$ stands for the $\Lambda\Lambda$ expectation value determined self-consistently, and $V_{\Lambda\Lambda}$ (SB) the two-range Gaussian potential given in the text. In $V_{\Lambda\Lambda}$ (SB) only the S -wave is used, while in the others converged results with enough partial waves are given.

$V_{\Lambda N}$	$V_{\Lambda\Lambda}$ (Hiyama)		FSS		fss2		$V_{\Lambda\Lambda}$ (SB)
	present	Ref. 42)	$\Delta B_{\Lambda\Lambda}$	$\varepsilon_{\Lambda\Lambda}$	$\Delta B_{\Lambda\Lambda}$	$\varepsilon_{\Lambda\Lambda}$	(S -wave)
SB	3.618	–	3.650	5.131	1.411	5.942	1.902
NS	3.548	3.59	3.623	5.159	1.364	5.951	1.917
ND	3.181	3.10	3.231	4.482	1.288	5.231	1.636
NF	3.208	3.22	3.301	4.626	1.270	5.410	1.719
JA	3.370	3.44	3.468	4.908	1.306	5.705	1.833
JB	3.486	3.56	3.592	5.150	1.325	5.956	1.924

shifts predicted by these interactions increase up to about 40° . The improved quark model fss2 yields $\Delta B_{\Lambda\Lambda} = 1.41$ MeV. (If we use the $\Lambda\Lambda$ single-channel T -matrix, this number is reduced to 1.14 MeV.) In Table IX, results are also shown for $V_{\Lambda\Lambda}$ (SB), which is a two-range Gaussian potential generated from the fss2 1S_0 $\Lambda\Lambda$ phase shift (see Fig. 11) in the full-channel calculation, using the supersymmetric inversion method.³⁹⁾ This potential is explicitly given by

$$V_{\Lambda\Lambda}(\text{SB}) = -103.9 \exp(-1.176 r^2) + 658.2 \exp(-5.936 r^2) ,$$

where $V_{\Lambda\Lambda}$ (SB) in MeV and r in fm is the relative distance between two Λ 's. We think that the 0.5 MeV difference between our fss2 result and the $V_{\Lambda\Lambda}$ (SB) result is probably because we neglected the full coupled-channel effects of the $\Lambda\Lambda\alpha$ channel to the $\Xi N\alpha$ and $\Sigma\Sigma\alpha$ channels. We should also keep in mind that in all of these three-cluster calculations the Brueckner rearrangement effect of the α -cluster with the magnitude of about -1 MeV (repulsive) is very important.²⁷⁾ It is also reported in Ref. 44) that the quark Pauli effect between the α cluster and the Λ hyperon yields a non-negligible repulsive contribution of 0.1 - 0.2 MeV for the Λ separation energy of $^6_{\Lambda\Lambda}\text{He}$, even when a rather compact ($3q$) size of $b = 0.6$ fm is assumed as in our quark-model interactions. Taking all of these effects into consideration, we can conclude that the present results by fss2 are in good agreement with the recent experimental value, $\Delta B_{\Lambda\Lambda}^{\text{exp}} = 1.01 \pm 0.20$ MeV, deduced from the Nagara event.²⁶⁾

§5. Summary

From the advent of Yukawa's meson theory, a huge amount of efforts have been devoted to understand the fundamental nucleon-nucleon (NN) interaction and related hadronic interactions. The present view of these interactions are non-perturbative realization of inter-cluster interactions, governed by the fundamental theory of the strong interaction, quantum chromodynamics (QCD), in which the gluons are the field quanta exchanged between quarks. On this basis, meson "the-

ory” can be understood as an effective description of quark-gluon dynamics in the low-energy regime. The short-range part of the NN and hyperon-nucleon (YN) interactions are still veiled with unaccessible mechanism of quark confinement and multi-gluon effects.

Here we have applied a naive constituent quark model to the study of baryon-baryon interactions, in which some of the essential features of QCD characteristics are explicitly incorporated in the non-relativistic framework. For example, the color degree of freedom of quarks is explicitly incorporated, and the full antisymmetrization of quarks is carried out in the resonating-group (RGM) formalism. The gluon exchange effect is represented in the form of the quark-quark interaction, for which a color analogue of the Fermi-Breit (FB) interaction is used with an adjustable parameter of the quark-gluon coupling constant α_S . The confinement potential is a phenomenological r^2 -type potential, which does not contribute to the baryon-baryon interactions in the present framework. Since the meson-exchange effects are the non-perturbative aspect of QCD, these are described by the effective meson exchange potentials (EMEP) acting between quarks. After several improvements, the most recent model called fss2 has achieved very accurate description of the NN and YN interactions.¹⁾⁻⁴⁾

We have extended this $(3q)$ - $(3q)$ RGM study of the the NN and YN interactions to the strangeness $S = -2$, -3 and -4 sectors without introducing any extra parameters, and have clarified some characteristic features of the B_8B_8 interactions.⁵⁾ The results seem to be reasonable, if we consider, i) the spin-flavor SU_6 symmetry, ii) the weak pion effect in the strangeness sector, and iii) the effect of the flavor symmetry breaking. These B_8B_8 interactions are now used for the detailed study of the few-body systems, as well as baryonic matter problems, in various ways. Here we discussed applications of the NN , YN and YY interactions to the Faddeev calculations of the three-nucleon bound state, the ΛNN - ΣNN system for the hypertriton, the $\alpha\alpha\Lambda$ system for ${}^9_\Lambda\text{Be}$, and the $\Lambda\Lambda\alpha$ system for ${}^6_{\Lambda\Lambda}\text{He}$. We find that fss2 gives the triton binding energy large enough to compare with the experiment, without reducing the deuteron D -state probability.^{7),29)} The charge root-mean-square radii of ${}^3\text{H}$ and ${}^3\text{He}$ are also correctly reproduced. The application to the hypertriton calculation shows that fss2 gives a reasonable result similar to the Nijmegen soft-core model NSC89,³⁵⁾ except for an appreciable contributions of higher partial waves.³¹⁾ In the application to the $\alpha\alpha\Lambda$ system, the $\alpha\alpha$ RGM kernel with the three-range Minnesota force³⁸⁾ and some appropriate ΛN force generated from the low-energy phase-shift behavior of fss2 yield the the ground-state and excitation energies of ${}^9_\Lambda\text{Be}$ within 100 - 200 keV accuracy.³⁷⁾ The weak $\Lambda\Lambda$ force $\Delta B_{\Lambda\Lambda}^{\text{exp}} = 1.01 \pm 0.20$ MeV deduced from the Nagara event²⁶⁾ for ${}^6_{\Lambda\Lambda}\text{He}$ is reasonably reproduced by the Faddeev calculation of the $\Lambda\Lambda\alpha$ system, using the present $\Lambda\alpha$ T -matrix and the full coupled-channel $\Lambda\Lambda$ - ΞN - $\Sigma\Sigma$ T -matrix of fss2.

It is important to note that the newly developed three-cluster Faddeev formalism using two-cluster RGM kernels opens a way to solve few-baryon systems interacting by the quark-model baryon-baryon interactions without spoiling the essential features of the RGM kernels; i.e., the non-locality, the energy dependence and the

existence of the pairwise Pauli-forbidden state. It can also be used for the three-cluster systems involving α -clusters, like the ${}^9_{\Lambda}\text{Be}$ and ${}^6_{\Lambda\Lambda}\text{He}$ systems. A nice point of this formalism is that the underlying NN and YN interactions are more directly related to the structure of the hypernuclei than the models assuming simple two-cluster potentials. In particular, we have found that the model fss2 yields a realistic description of many three-body systems including the three-nucleon bound state, the hypertriton, ${}^9_{\Lambda}\text{Be}$ and ${}^6_{\Lambda\Lambda}\text{He}$.

Acknowledgements

This work was supported by Grants-in-Aid for Scientific Research (C) (Nos. 15540270, 15540284 and 15540292) and for Young Scientists (B) (No. 15740161) from the Japan Society for the Promotion of Science (JSPS).

References

- 1) Y. Fujiwara, C. Nakamoto and Y. Suzuki, Phys. Rev. Lett. **76** (1996), 2242.
- 2) Y. Fujiwara, C. Nakamoto and Y. Suzuki, Phys. Rev. C **54** (1996), 2180.
- 3) T. Fujita, Y. Fujiwara, C. Nakamoto and Y. Suzuki, Prog. Theor. Phys. **100** (1998), 931.
- 4) Y. Fujiwara, T. Fujita, M. Kohno, C. Nakamoto and Y. Suzuki, Phys. Rev. C **65** (2002), 014002.
- 5) Y. Fujiwara, M. Kohno, C. Nakamoto and Y. Suzuki, Phys. Rev. C **64** (2001), 054001.
- 6) M. Kohno, Y. Fujiwara, T. Fujita, C. Nakamoto and Y. Suzuki, Nucl. Phys. A **674** (2000), 229.
- 7) Y. Fujiwara, K. Miyagawa, M. Kohno, Y. Suzuki and H. Nemura, Phys. Rev. C **66** (2002), 021001.
- 8) Y. Fujiwara, H. Nemura, Y. Suzuki, K. Miyagawa and M. Kohno, Prog. Theor. Phys. **107** (2002), 745.
- 9) Y. Fujiwara, Y. Suzuki, K. Miyagawa, M. Kohno and H. Nemura, Prog. Theor. Phys. **107** (2002), 993.
- 10) Y. Fujiwara, M. Kohno, T. Fujita, C. Nakamoto and Y. Suzuki, Prog. Theor. Phys. **103** (2000), 755.
- 11) Y. Fujiwara, M. Kohno, C. Nakamoto and Y. Suzuki, Prog. Theor. Phys. **104** (2000), 1025.
- 12) R. A. Arndt, Scattering Analysis Interactive Dial-up (SAID), Virginia Polytechnic Institute, Blacksburg, Virginia (private communication).
- 13) O. Dumbrajs *et al.*, Nucl. Phys. B **216** (1983), 277.
- 14) N. L. Rodning and L. D. Knutson, Phys. Rev. C **41** (1990), 898.
- 15) David M. Bishop and Lap M. Cheung, Phys. Rev. A **20** (1979), 381.
- 16) I. Lindgren, in *Alpha-, Beta- and Gamma-Ray Spectroscopy*, edited by K. Siegbahn, Vol. II, (North-Holland, Amsterdam, 1965), p. 1621.
- 17) M. Lacombe, B. Loiseau, J. M. Richard, R. Vinh Mau, J. Côté, P. Pirès and R. de Tournell, Phys. Rev. C **21** (1980), 861.
- 18) R. Machleidt, Adv. Nucl. Phys. **19** (1989), 189.
- 19) R. Brockmann and R. Machleidt, Phys. Rev. C **42** (1990), 1965.
- 20) Th. A. Rijken, V. G. J. Stoks and Y. Yamamoto, Phys. Rev. C **59** (1999), 21.
- 21) Y. Kondo *et al.* (KEK-PS E289 collaboration), Nucl. Phys. A **676** (2000), 371.
- 22) J. K. Ahn *et al.* (KEK-PS E251 collaboration), Nucl. Phys. A **648** (1999), 263.
- 23) T. Kadowaki *et al.* (KEK-PS E452 collaboration), Eur. Phys. J. **A15** (2002), 295.
- 24) T. Tamagawa *et al.* (BNL-E906 collaboration), Nucl. Phys. A **691** (2001), 234c.
- 25) Y. Yamamoto, T. Tamagawa, T. Fukuda and T. Motoba, Prog. Theor. Phys. **106** (2001), 363.
- 26) H. Takahashi *et al.* (KEK-PS E373 collaboration), Phys. Rev. Lett. **87** (2001), 212502.
- 27) M. Kohno, Y. Fujiwara and Y. Akaishi, Phys. Rev. C **68** (2003), 034302.
- 28) V. G. J. Stoks and Th. A. Rijken, Phys. Rev. C **59** (1999), 3009.
- 29) Y. Fujiwara, K. Miyagawa, Y. Suzuki, M. Kohno and H. Nemura, Nucl. Phys. A **721**

- (2003), 983c.
- 30) A. Nogga, H. Kamada and W. Glöckle, Phys. Rev. Lett. **85** (2000), 944.
 - 31) Y. Fujiwara, K. Miyagawa, M. Kohno and Y. Suzuki, KUNS-1907, nucl-th/0404010, submitted to Phys. Rev. C.
 - 32) K. Miyagawa, H. Kamada, W. Glöckle and V. Stoks, Phys. Rev. C **51** (1995), 2905.
 - 33) K. Miyagawa, H. Kamada, W. Glöckle, H. Yamamura, T. Mart and C. Bennhold, Few-Body Systems Suppl. **12** (2000), 324.
 - 34) A. Nogga, H. Kamada and W. Glöckle, Phys. Rev. Lett. **88** (2002), 172501.
 - 35) P. M. M. Maessen, Th. A. Rijken and J. J. de Swart, Phys. Rev. C **40** (1989), 2226.
 - 36) H. Nemura, Y. Akaishi and Y. Suzuki, Phys. Rev. Lett. **89** (2002), 142504.
 - 37) Y. Fujiwara, K. Miyagawa, M. Kohno, Y. Suzuki, D. Baye and J.-M. Sparenberg, KUNS-1910, nucl-th/0404071, submitted to Phys. Rev. C.
 - 38) D. R. Thompson, M. LeMere and Y. C. Tang, Nucl. Phys. A **286** (1977), 53.
 - 39) J.-M. Sparenberg and D. Baye, Phys. Rev. C **55** (1997), 2175.
 - 40) R. H. Dalitz, R. C. Herndon and Y. C. Tang, Nucl. Phys. B **47** (1972), 109.
 - 41) H. Bando and I. Shimodaya, Prog. Theor. Phys. **63** (1980), 1812.
 - 42) E. Hiyama, M. Kamimura, T. Motoba, T. Yamada and Y. Yamamoto, Prog. Theor. Phys. **97** (1997), 881.
 - 43) H. Aikawa *et al.* (BNL-E930 collaboration), Phys. Rev. Lett. **88** (2002), 082501.
 - 44) Y. Suzuki and H. Nemura, Prog. Theor. Phys. **102** (1999), 203.